KeAi

CHINESE ROOTS
GLOBAL IMPACT

Contents lists available at ScienceDirect

Petroleum Science

journal homepage: www.keaipublishing.com/en/journals/petroleum-science



Original Paper

Evaluation of hydraulic fracturing of horizontal wells in tight reservoirs based on the deep neural network with physical constraints



Hong-Yan Qu ^{a, b, c, *}, Jian-Long Zhang ^{a, c}, Fu-Jian Zhou ^{a, b, c}, Yan Peng ^d, Zhe-Jun Pan ^e, Xin-Yao Wu ^f

- ^a State Key Laboratory of Petroleum Resources and Prospecting, China University of Petroleum, Beijing, 102249, China
- ^b School of Artificial Intelligence, China University of Petroleum, Beijing, 102249, China
- ^c Unconventional Oil and Gas Institute, China University of Petroleum, Beijing, 102249, China
- ^d School of Petroleum Engineering, China University of Petroleum, Beijing, 102249, China
- ^e Key Laboratory of Continental Shale Hydrocarbon Accumulation and Efficient Development, Ministry of Education, Northeast Petroleum University, Daging, Heilongjiang, 163318, China
- f Engineering Technology Research Institute, PetroChina Xinjiang Oilfield Company, Karamay, Xinjiang, 834000, China

ARTICLE INFO

Article history: Received 16 January 2023 Received in revised form 24 February 2023 Accepted 17 March 2023 Available online 20 March 2023

Edited by Jia-Jia Fei

Keywords:
Evaluation of fracturing effects
Tight reservoirs
Physical constraints
Deep neural network
Horizontal wells
Combined neural network

ABSTRACT

Accurate diagnosis of fracture geometry and conductivity is of great challenge due to the complex morphology of volumetric fracture network. In this study, a DNN (deep neural network) model was proposed to predict fracture parameters for the evaluation of the fracturing effects. Field experience and the law of fracture volume conservation were incorporated as physical constraints to improve the prediction accuracy due to small amount of data. A combined neural network was adopted to input both static geological and dynamic fracturing data. The structure of the DNN was optimized and the model was validated through k-fold cross-validation. Results indicate that this DNN model is capable of predicting the fracture parameters accurately with a low relative error of under 10% and good generalization ability. The adoptions of the combined neural network, physical constraints, and k-fold cross-validation improve the model performance. Specifically, the root-mean-square error (RMSE) of the model decreases by 71.9% and 56% respectively with the combined neural network as the input model and the consideration of physical constraints. The mean square error (MRE) of fracture parameters reduces by 75% because the k-fold cross-validation improves the rationality of data set dividing. The model based on the DNN with physical constraints proposed in this study provides foundations for the optimization of fracturing design and improves the efficiency of fracture diagnosis in tight oil and gas reservoirs. © 2023 The Authors. Publishing services by Elsevier B.V. on behalf of KeAi Communications Co. Ltd. This is an open access article under the CC BY-NC-ND license (http://creativecommons.org/licenses/by-nc-nd/

4.0/).

1. Introduction

Horizontal well with volumetric fracturing is the key technology for the commercial development of tight oil and gas reservoirs (Lei et al., 2022). The staggered well design and zipper fracturing technology were adopted to develop the vertical superimposed multi-layers (Jaripatke et al., 2018). This improves oil and gas production in some oilfields in the western China (Lei et al., 2021; Li et al., 2020). However, the complex morphology of the multi-layer fracture network leads to significant challenges of hydraulic fracturing evaluation.

E-mail address: hongyan.qu@cup.edu.cn (H.-Y. Qu).

Fracture geometry and conductivity need to be accurately diagnosed for the optimization of stimulation measures. It is more difficult for the three-dimensional well platform due to more wells, fracturing stages and perforation clusters. The common methods of fracture diagnosis include direct monitoring and indirect inversion. The direct monitoring technologies include tracer monitoring, microseismic monitoring, surface or downhole inclinometer, and optical fiber monitoring (Li et al., 2019, 2020; Li et al., 2020; Liu et al., 2020; Miao et al., 2019; Pakhotina et al., 2020; Tian et al., 2016; Zhou et al., 2015). However, these technologies could not be widely applied due to the short migration distance of tracer, low signal-to-noise ratio and high cost (Mahmoud et al., 2021). In addition, fracture conductivity could not be obtained through these methods in addition to the fracture geometry.

Apart from the direct monitoring, the indirect inversion is another common method for fracture diagnosis, such as Diagnostic

^{*} Corresponding author. State Key Laboratory of Petroleum Resources and Prospecting, China University of Petroleum, Beijing, 102249, China.

Fracture Injection Tests (DFITs) (Barree et al., 2009; Wallace et al., 2016), numerical simulation (Yang et al., 2017), fracture model analysis (Fiallos Torres et al., 2021; Fries and Belytschko, 2010; Shauer and Duarte, 2019), and production history matching (Soleimani, 2017; Xiao et al., 2021). These methods are more suitable for conventional reservoirs whereas the fracture parameters interpreted in tight reservoirs may often deviate from the real values. These discrepancies may result from complexity of fracture morphology and ideal assumption of the inversion model (Mahmoud et al., 2021).

To sum up, more time and efforts are needed to obtain accurate fracture geometry parameters with the direct and indirect diagnosis methods. It is difficult to diagnose complex fractures for the three-dimensional horizontal well fracturing. However, a large amount of data has been accumulated in tight oil and gas reservoirs in recent years due to the wide application of horizontal well fracturing technology. The utilization of data-driven machine learning could possibly be a new solution.

Great efforts have been put on the application of machine learning and the developed deep neural network (DNN), known as deep learning (DL), in the oil industry (He et al., 2021; Huang et al., 2020; Liu et al., 2020; Sang et al., 2021). The improved algorithms (such as convolutional neural network (CNN)) have been applied to data processing and parameter prediction of fractured wells because of strong learning ability (Janiesch et al., 2021). Specifically, the DL method was applied in the production prediction, rapid optimization of horizontal well parameters and reservoir characteristic description (Kulga et al., 2018). It has also been applied to microseismic event processing and production history matching (Chen and Saad, 2022; Tripoppoom et al., 2020; Wang et al., 2022; Zhang et al., 2018).

Most of the applications were pure data driven, whereas there are some problems with the data. Noteworthily, there are much accumulated experimental and numerical data while some data are invalid and could not be used. In contrast, the data available for some specific problems is not enough to support pure data-driven deep learning. In addition, the pure data-driven models are often impractical without physical meaning. Therefore, the prediction accuracy of the pure data-driven model with small amount of valid data is poor.

The physics-informed neural networks (PINN) improves the prediction accuracy of the DL model in two ways. The mathematical equations including controlling equations, boundary conditions, and initial conditions can be converted to loss functions. In particular, the productivity equation could be added to the loss function to predict well production to form physically constrained deep learning frameworks (Dong et al., 2022). Different types of loss functions could be applied to guide the training process of seismic impedance inversion. The fracturing effect of coalbed methane reservoirs could be evaluated with data-driven model with physical laws (Song et al., 2022).

Alternatively, the physical models can be transformed to the components of neural networks. Specifically, the rock physics model was regarded as the activation function of convolutional neurons to predict the overpressure (Cheng and Fu, 2022). The porosity and specific surface area were incorporated into the secondary network to predict permeability through digital core images (Wu et al., 2018). In short, the PINN has been mostly applied to the production prediction, while greater challenges of data collecting, model optimization and physical constrains have been proposed for the evaluation of the fracturing effects of horizontal wells.

In this study, a PINN model was proposed to evaluate the fracturing effects of horizontal wells in tight oil and gas reservoirs. Field experience and physical model were incorporated as physical constraints. In addition, the evaluation model was optimized and validated to improve prediction accuracy. Moreover, the effects of the combined neural network, physical constraints, and k-fold cross-validation method on the performance of the model were analyzed. Furthermore, the model was utilized to predict the fracturing parameters of the well in adjacent platform to prove generalization ability of the model. The establishment of the evaluation model of fracturing effects for horizontal wells in tight reservoirs provides foundations for the real-time optimization of fracturing parameters and maximization of economic benefits.

2. Methodology

2.1. Deep neural network

In this study, the deep neural network is the critical component of the evaluation model of the fracturing effect of horizontal wells to extract features from input data and acquire evaluation parameters through model optimization and validation. The Deep Neural Network (DNN) was developed on the basis of Artificial Neural Network (ANN) (Shrestha and Mahmood, 2019). Different from ANN with only one hidden layer, there are multiple hidden layers in DNN, which greatly improves the ability of DNN to extract data features (Syed et al., 2022). In addition, the DNN model performs better on model convergence and parameter adjustment, compared with conventional neural networks (such as BP neural networks).

2.2. Combined neural network

Appropriate neural networks need to be selected according to different types of input data of the evaluation model of fracturing effects of horizontal wells (Valle dos Santos and Vellasco, 2015). The conventional neural network is suitable to process onedimensional data, while the convolutional neural networks are suitable for two-dimensional and three-dimensional data. Single neural network does not perform well with different data dimensions, and several networks need to be combined together to input data. In this study, the input data consist of one-dimensional geological data and two-dimensional fracturing treatment data, considered as static data and dynamic data respectively according to whether they change with time. Since the amount of dynamic data is much larger than that of the static data, the characteristics of the dynamic data would be more highlighted if only one neural network was used to input data, resulting in insufficient utilization of input data. Therefore, two deep neural networks with different dimensions were combined into a new neural network, which was utilized in this study to input data according to the characteristics of both dynamic and static data, solving the problem of inconsistent dimensions of input data.

2.3. Deep neural network with physical constraints

Since the amount of the sample data of the hydraulic fracturing evaluation is relatively small, the prediction results with conventional deep neural networks may deviate from the real ones due to the lack of physical meaning. The introduction of physical constraints into the deep neural network can effectively solve this problem. In this study, physical constraints were incorporated into the loss function of the deep neural network, which measures the deviation between the prediction of the model and the real value, to restrain the prediction results. The model training and test are to minimize the model loss.

The loss function of the conventional data-driven model can be expressed with the mean square error (MSE) as follows:

$$MSE = \frac{1}{N} \sum_{i=1}^{N} \left(y_i^{\text{predict}} - y_i^{\text{data}} \right)^2$$
 (1)

where MSE represents the mean square error, N represents the number of sample data, y_i^{predict} is the predicted value, and y_i^{data} is the true value.

In this study, the field experience, namely the fracturing parameters estimated by oilfield experts according to the geological data and fracturing treatment data, was supplemented into the loss function to further improve the prediction accuracy of the model. The prediction results of the model should be within the probable ranges of the fracture parameters given by the field experience. The loss function of the field experience can be described as follows:

$$Loss_{f} = \begin{cases} 0, \langle y_{fj\min} \leq y_{fij}^{\text{predict}} \leq y_{fj\max} \rangle \\ y_{fij}^{\text{predict}} + \left(y_{fj\max} + y_{fj\min} \right) / 2, \langle \text{else} \rangle \end{cases}$$
 (2)

$$Loss_{k} = \begin{cases} 0, \langle y_{k\min} \leq y_{ki}^{\text{predict}} \leq y_{k\max} \rangle \\ y_{ki}^{\text{predict}} + (y_{k\max} + y_{k\min}) / 2, \langle \text{else} \rangle \end{cases}$$
(3)

where *Loss* represents the loss defined by the field experience, the subscript f represents the fracture geometry, the subscript k represents the fracture permeability, y_f^{predict} represents the predicted fracture geometry parameters, y_k^{predict} represents the predicted fracture permeability, $y_{f\text{min}}$ and $y_{f\text{max}}$ represents the minimum and maximum value of the fracture geometric parameters respectively according to the field experience, $y_{k\text{min}}$ and $y_{k\text{max}}$ represents the minimum and maximum value of the fracture permeability respectively according to the field experience, j=1,2,3 represents the fracture length, fracture height, and fracture width respectively, and i represents the number of the data samples.

Apart from the field experience, a two-dimensional fracture geometry calculation model was also considered as a part of the physical constraints. The common two-dimensional fracture models include the PKN model and the KGD model (Esfandiari and Pak, 2023). The fracture width and fracture length of the KGD model were selected as other physical constraints of the neural network model considering the impact of filtration on fracture propagation. The difference between the prediction results of the DNN model and the calculation results of the KGD model is regarded as a part of the loss function. The model was trained according to the model loss, and the calculation results of the KGD model were used to constrain the model to avoid the unreasonable prediction from the deep neural network model. The fracture width and length of the KGD fracture model were calculated as follows:

$$w = 1.87 \left[\frac{(1 - \nu)q^3 \mu}{G} \right]^{\frac{1}{6}} t^{1/3}$$
 (4)

$$L = 0.68 \left[\frac{Gq^3}{(1-v)\mu} \right]^{\frac{1}{6}} t^{2/3}$$
 (5)

where w is the fracture width, L is the fracture length, ν is the Poisson's ratio of the rock, q is the slurry rate, μ is the viscosity of the fracturing fluid, G is the shear modulus of the rock, and t is the fracturing treatment time.

The loss function of the KGD fracture model is described as follows:

$$Loss_{2D} = y_{f i,1}^{\text{predict}} - L_i + y_{f i,3}^{\text{predict}} - w_i$$
 (6)

where $Loss_{\rm 2D}$ represents the loss of the two-dimensional fracture model, $y_{f,1}^{\rm predict}$ and $y_{f,3}^{\rm predict}$ represents the fracture length and width predicted by the model respectively, and w and L represents the fracture width and fracture length calculated by the KGD model respectively.

The total loss function was obtained by combining the loss functions of the data-driven model, field experience, and fracture model (Song et al., 2022), and expressed as follows:

$$Loss_{all} = \alpha_1 RMSE + \alpha_2 \frac{1}{N} \sum_{i=1}^{N} \left(Loss_f + Loss_k \right) + \alpha_3 \frac{1}{N} \sum_{i=1}^{N} (Loss_{2D})$$
 (7)

where $Loss_{all}$ represents the total loss, α_1 , α_2 and α_3 represents the weight coefficient for each specific loss respectively, and the specific value needs to be verified through model training.

3. Procedure

3.1. Workflow

In this study, the evaluation model of the fracturing effect of horizontal wells was established based on the deep neural network with physical constraints. The specific workflow includes the establishment of sample data set, construction of the evaluation model, model optimization, model validation and fracturing effect evaluation, as shown in Fig. 1. The optimized and validated model can be used to evaluate the fracturing effect of horizontal wells, and the fracture geometry parameters and fracture permeability can be predicted by inputting geological data and fracturing treatment data

The sample data set was established with a total of 200 samples selected, including both input and output data. The input data are composed of geological data (static data) and fracturing treatment data (dynamic data). The geological data were obtained through calculation with logging data. The fracturing treatment data were

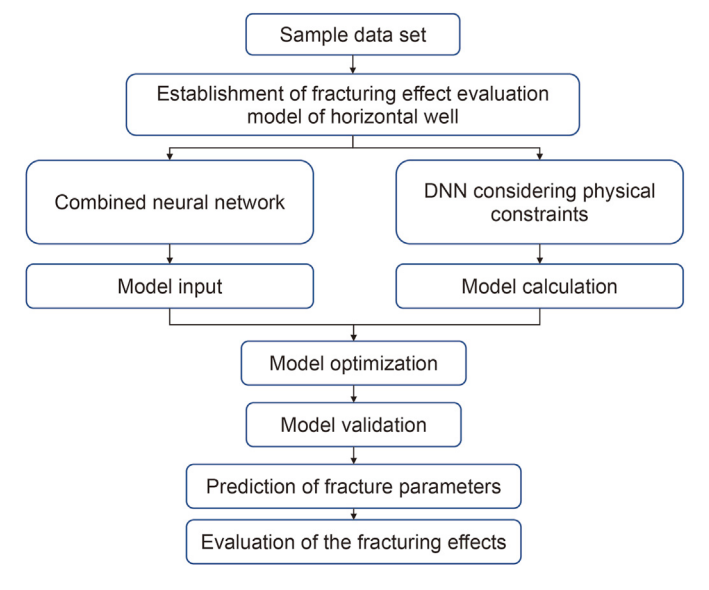


Fig. 1. The workflow chart of the establishment of the evaluation model of fracturing effects of horizontal wells.

preprocessed to obtain the fracturing treatment data table with the same dimension. The output data include fracture geometry parameters (fracture length, fracture width and fracture height) and fracture permeability, which were obtained through fracturing pressure fitting and verified with microseismic data to ensure the reliability of the sample data.

In addition, the evaluation model of the fracturing effect was established based on the sample data, composed of a combined neural network and a deep neural network. The combined neural network was constructed with different neurons assigned to each neural network according to the characteristics of the input dynamic data and static data. In this way, the two different types of data were effectively input into the model. The combined neural network was connected to the deep neural network and the physical constraints were considered by redefining the loss function to improve the prediction accuracy with small sample data. The parameters of the deep neural network model were initialized, and the data set was divided into the training set and test set for the model calculation.

Moreover, the model was optimized through optimizing the number of hidden layers of the deep neural network and the number of neurons in each hidden layer according to the model calculation results, and further validated with the *k*-fold cross-validation by re-dividing the data set. The effects of hydraulic fracturing were evaluated based on the predicted fracture parameters.

Furthermore, the impacts of the combined neural network, physical constraints, and k-fold cross-validation on the evaluation model of the fracturing effect of horizontal wells were analyzed, and the model was applied to predict the fracture parameters of the other wells in adjacent platforms.

3.2. Establishment of the sample data set

The sample data in this study is derived from a tight oil reservoir in western China. A set of three-dimensional staggered well pattern is designed in platform A in X region, and eight wells are deployed in two adjacent layers. The intralayer and interlayer well spacing is 200 m and 100 m respectively, and the length of each horizontal well is 1800 m. The collected data include geological data and fracturing treatment data of 380 stages of the 8 fractured horizontal wells on the platform in the reservoir. Data of 200 stages were selected as the sample data in this study after invalid data were eliminated due to sand plugging or other operating problems.

The sample data of the model includes both input and output data. The input data consists of static geological data and dynamic fracturing data. The geological data of each fracturing stage of the wells were obtained by calculating the average value of the geological parameters according to the depth of the stage with the logging data. Fracturing treatment data were recorded in the process of fracturing treatments, which change with time. The output data are composed of fracture geometry parameters (fracture length, fracture width, and fracture height) and fracture permeability, which were obtained by fitting the fracturing treatment pressure of each stage of the horizontal wells.

3.2.1. Preparation of static input data

The fracture geometry parameters are affected by the geomechanical parameters, such as reservoir pressure, the maximum and minimum horizontal principal stress, Young's modulus and Poisson's ratio. Fracture permeability is related to the permeability, porosity and oil saturation in the reservoir. Therefore, these controlling parameters were selected as the input geological data,

which were calculated with logging data and averaged by depth. The mean data of each fracturing stage were selected as the geological data for that stage. The detailed ranges and values of the static input data are shown in Table 1.

3.2.2. Preprocessing of dynamic input data

The geological data can be directly input into the model, while the fracturing data need to be processed in advance. Three parameters affecting fracture propagation were selected as the components of dynamic data, including fracturing treatment pressure, sand concentration and pumping rate. Since the fracturing data were monitored and recorded in seconds in the process of fracturing treatment, the amount of data in each horizontal well is large with different time steps for different fracturing stages. In addition, the pressure test data before fracturing is not very relevant to the fracture propagation, as shown in Fig. 2a. The redundant and inconsistent data of each stage increases the difficulty of training the neural network, and need to be preprocessed through effective fracturing data selecting, data denoising, and feature point extraction.

(1) Fracturing data tailoring

The high-viscosity slick water was utilized as the pad fluid to initiate fractures, which was denoted by the amount of liquid addition in the pumping schedule. The effective fracturing data starts when the amount of liquid addition is over 0 for the first time. Therefore, the amount of liquid addition was chosen as an index to retain the effective fracturing treatment data.

Taking the fracturing data of stage S of well B as an example, effective fracturing data were obtained after the original fracturing treatment data were tailored, as shown in Fig. 2a, and the pressure and pumping rate of the effective fracturing data no longer start from 0. In addition, the amount of data after tailoring drops from 8000 to under 7000, reducing the time and difficulty of model training, and saving the training memory of the neural network. The data of other fracturing stages in all wells were processed and effective fracturing data were obtained in the same way.

(2) Data denoising

The signals of downhole pressure and temperature collected from hydraulic fracturing are normally with noise, which needs to be removed and valid signals need to be retained. The fracturing pressure fluctuates, as shown in Fig. 2b. The drastic fluctuations may result from fracture initiation and fracture closure while the small ones may be induced by the noise. Therefore, the fracturing data needs to be denoised before feature points were extracted.

The fracturing pressure is mainly denoised because it is affected by the change of pumping rate, proppant concentration and fracturing fluid viscosity during the fracturing treatment. A great many of methods have been developed for signal denoising based on the spectral distribution and statistical characteristics of the noise, among which the wavelet denoising method is more commonly used. In this study, the wavelet denoising toolbox in the software of MATLAB was utilized to process the fracturing pressure data. Proper denoising methods were selected according to the indicators of signal-to-noise ratio (SNR) and root-mean-square error (RMSE). The effectiveness of the wavelet denoising was evaluated by the indicator of smoothness (r). Generally, the larger the SNR and the smaller the RMSE and r, the smoother the signals, and the better the denoising effect. The indicators of SNR, RMSE and r can be expressed as follows:

Table 1The static input data of the model.

Variables	Parameters	Туре	Range	Mean	Unit
Reservoir geological data	Reservoir Pressure	point	49.29-52.37	50.8987	MPa
	Maximum horizontal stress	point	63.82-102.72	82.48	MPa
	Minimum horizontal stress	point	54.53-78.73	69.12	MPa
	Poisson's ratio	point	0.27-0.29	0.28	1
	Young's modulus	point	16.7-21.83	20.8	GPa
	Oil saturation	point	0.77-0.89	0.82	%
	Porosity	point	0.12-0.175	0.15	1
	Permeability	point	0.001-3.3	0.0336	mD

$$SNR = 10 \times \lg\left(\frac{1}{n}\sum_{n}f^{2}(n) / \frac{1}{n}\sum_{n}\left[f(n) - \hat{f}(n)\right]^{2}\right)$$
 (8)

RMSE =
$$\sqrt{\frac{1}{n} \sum_{i=1}^{n} \left[f(i) - \hat{f}(i) \right]^2}$$
 (9)

$$r = \sum_{i=1}^{n-1} \left[\hat{f}(i+1) - \hat{f}(i) \right]^2 / \sum_{i=1}^{n-1} \left[f(i+1) - f(i) \right]^2$$
 (10)

where f(i) represents the original signal, f(i) represents the signal after denoising, n represents the number of signals, and i represents the ith signal.

Specifically, the biorthogonal spline wavelets were selected as the wavelet family to distinguish weak signals, and Stein's Unbiased Risk Estimate was selected as the noise reduction method in the process of denoising fracturing pressure data. The soft threshold constraint was used to decompose the 10-layer signals to obtain the denoised pressure data. The results indicate that the fracturing pressure data curve is effectively smoothed with the denoising indicators SNR, RMSE and r of 145.68, 0.0018, and 0.9903 respectively, and the effective feature points are retained. As shown in Fig. 2b, the slight fluctuations of the fracturing pressure in the red circle are replaced by the smooth data, while the turning points with larger fluctuations in the blue circle are preserved.

(3) Feature point extraction

The data amount needs to be maintained the same for each fracturing stage for the consistency of dimensions of the model input data. However, different fracturing treatment time results in the difference in data amount for each fracturing stage. Therefore, a certain number of feature points of the fracturing data should be selected for each fracturing stage, determined by the prediction errors of the neural network model. In this study, the intersection of corresponding pressure points where proppant concentration and fracturing pressure exceeds a certain threshold respectively were regarded as the feature pressure points as follows:

$$P\{P_1, P_2, ... P_X\} = P_i (\Delta N_{\text{proppant}} \ge a) \cap P_i (\Delta P \ge b) (i = 1, 2, ... n)$$
(11)

where $P\{P_1, P_2, ... P_X\}$ represents the feature pressure points, $\Delta N_{\text{proppant}}$ represents the change of proppant concentration, ΔP represents the change of pressure, a and b are the threshold values, and n is the number of data points in each fracturing stage.

The threshold of proppant concentration and fracturing pressure was determined by the average of the difference between two adjacent values respectively. The pumping rates and the proppant

concentrations corresponding to these feature pressure points were also selected as the input data. The fracturing pressure, pumping rate and proppant concentration of each selected time step form a X*1 data table respectively as the input dynamic data of the combined neural network. The dynamic data are detailed in Table 2.

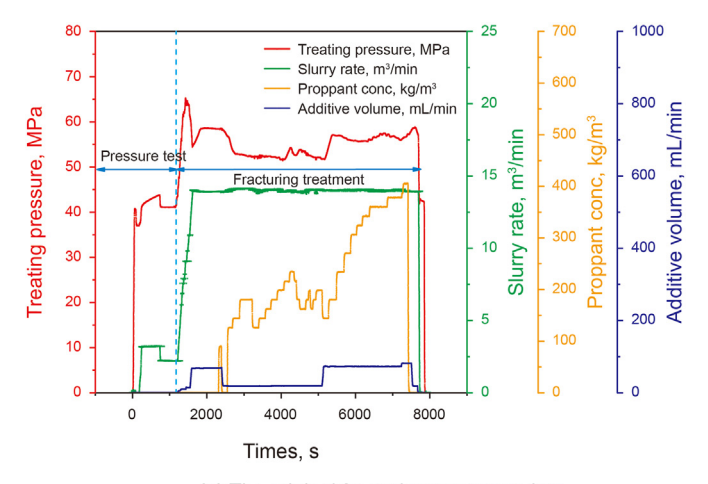
Results indicate that the number of feature points has great impacts on the model performance. As the number increases, the amount of information extracted from the data increases, and the RMSE of the model gradually decreases, as shown in Fig. 2c. The smaller the number of feature points, the more the data loss and the worse the prediction. Specifically, the RMSE decreases by 2.14 when the number of feature points increases from 2000 to 4000. The number of feature points is determined to be 2000 after comprehensive evaluation. The amount of input dynamic data reduces from 7897 to 2000 after preprocessing, much smaller than the original amount, while the important features of the original data are maintained.

3.2.3. Preparation of the evaluation parameters of fracturing effects

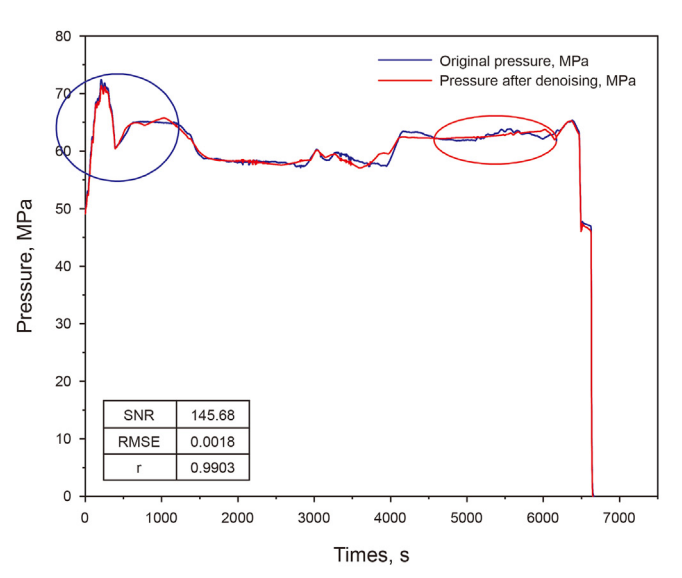
The fracture parameters including the fracture length, fracture height, fracture width, and fracture conductivity need to be predicted to evaluate the hydraulic fracturing effects. Since the fracture conductivity is the multiplication of fracture width and fracture permeability, the fracture length, fracture height, fracture width and fracture permeability were set as the evaluation parameters of the fracturing effect, which are also the output of the neural network model.

Since the fracture parameters cannot be directly obtained from the field monitoring (Zhao et al., 2022), they were inverted with the common method of fracturing pressure analysis in this study. The fracture geometric parameters and fracture conductivity were determined by applying and combining the flow equation, continuity equation and the fracture calculation model during fracturing treatment and after pump stopping. The fracturing treatment pressures of each fracturing stage were analyzed and fitted with the geomechanical model and the fracturing treatment scheme using the software of Petrel. In addition, the in-situ stress and frictions caused by fracturing fluid and proppant were corrected, and the parameters including fracture length, fracture height, fracture width and fracture permeability were obtained through inversion. Moreover, the inverted fracture parameters were compared with the field microseismical data to ensure the accuracy of the inversion and the reliability of the model output data.

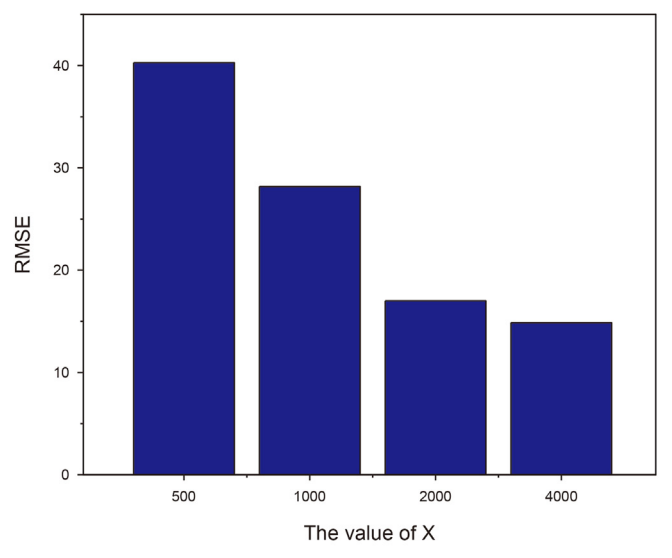
The fracture parameters obtained through inversion are well matched with the field microseismic data, as shown in Fig. 3. Taking the 39 fracturing stages of well B in platform A as an example, the MRE between the inverted fracture length and the microseismic data is 0.053, and the correlation coefficient (R^2) is over 0.8, indicating that these parameters are relatively valid as the output data of the model. All sample output data of the evaluation model were obtained in this way.



(a) The original fracturing treatment data



(b) Comparison of fracturing pressure before and after wavelet denoising



(c) Comparison of RMSE for different numbers of feature points

Fig. 2. Preprocessing of fracturing treatment data of stage S of well B in platform A.

3.3. Establishment of the model of fracturing effect evaluation of horizontal well

The model of fracturing effect evaluation of horizontal wells was established in this section, which is composed of a combined neural network and a deep neural network, as shown in Fig. 4. The function of the combined neural network is to input data reasonably according to the data characteristics, while the deep neural network focuses on model calculation and prediction.

The deep neural network consists of one input layer, one output layer, three hidden layers and physical constraints. There are 300 neurons in each hidden layer. The physical constraints are characterized with the loss function composed of the conventional datadriven loss function, field experience, and physical model.

The combined neural network is composed of two neural networks in parallel. The first neural network is composed of one layer of neural network containing eight neurons to input the geological data including reservoir pressure, the maximum and minimum horizontal principal stress, Poisson's ratio, Young's modulus, porosity, permeability, and oil saturation. The second neural network consists of one input layer, six hidden layers and one output layer, through which hydraulic fracturing treatment data are input. The input layer is constructed by allocating 2000 neurons to the fracturing treatment pressure, proppant concentration and pumping rate respectively. Six hidden layers are set for the second neural network because the amount of hydraulic fracturing treatment data is much larger than that of the geological data, and the impact of geological data on the model results may be weakened during model calculation, 800 neurons are contained in each hidden layer, and 100 neurons are contained in the output layer. In this way, the large fracturing data can be compressed to 100 neurons without modifying the initial data, reducing the excessive impact of the fracturing data on the model.

The evaluation indicators including the root-mean-square error (RMSE), mean relative error (MRE) and correlation coefficient (R^2) were employed to evaluate the performance of the model, which were calculated as follows:

$$RMSE = \sqrt{\frac{1}{N} \sum_{i=1}^{N} (y_i^{perdict} - y_i^{data})^2}$$
 (12)

$$MRE = \frac{1}{n} \sum_{i=1}^{n} \frac{\left| y_i^{\text{predict}} - y_i^{\text{data}} \right|}{y_i^{\text{data}}}$$
 (13)

$$R^{2} = 1 - \frac{\sum_{i=1}^{n} \left(y_{i}^{\text{predict}} - y_{i}^{\text{data}} \right)^{2}}{\sum_{i=1}^{n} \left(\text{average} \left(y_{i}^{\text{data}} \right) - y_{i}^{\text{data}} \right)^{2}}$$

$$(14)$$

where y_i^{predict} is the predicted value, y_i^{data} is the real data or true value, n is the number of sample data, and $\text{average}(y_i^{\text{data}})$ is the average value of the true value.

The fracturing effects of the horizontal wells can be evaluated based on the predicted fracture parameters. In this study, the stimulated reservoir volume (SRV) (Cipolla et al., 2008), fracture complexity index (FCI) and fracture conductivity (FC) were selected as the evaluation indicators of fracturing effects. They are calculated as follows:

Table 2Dynamic input data parameters of the model.

Variables	Parameters	Type	Range	Mean	Unit
Hydraulic fracturing data	Treatment pressure	table	0-80		MPa
	Pumping rate	table	0-16		m³/min
	Proppant concentration	table	0-400		kg/m³

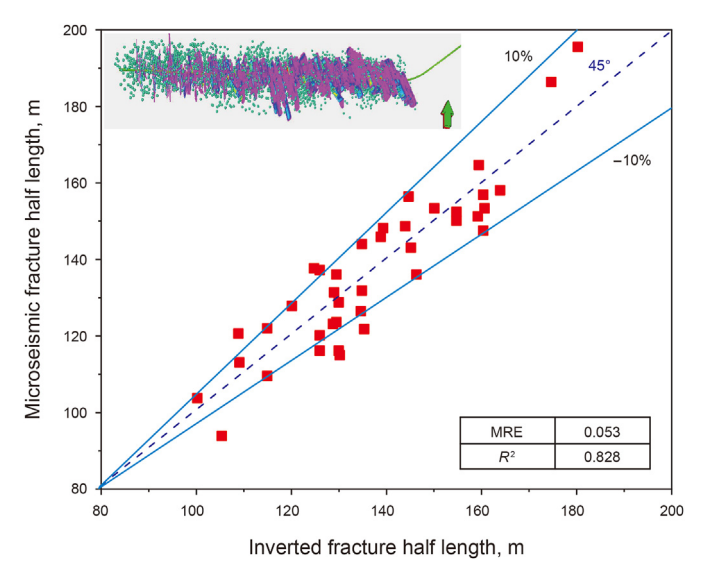


Fig. 3. Comparison of inverted fracture length and microseismic data in 39 fracturing stages of Well B in Platform A (the superposition diagram of two-dimensional fracture inversion and microseismic data were illustrated in the upper left corner. The rose red color represents the inverted fracture, and the green points are microseismic data).

$$SRV = \sum_{i=1}^{n} 2L_{f,i} \times 2W_i \times H_i \times \sin \alpha_i$$
 (15)

$$FCI = \frac{\sum_{i=1}^{n} W_i / L_{f,i}}{n}$$
 (16)

$$FC = \frac{\sum_{i=1}^{n} W_{f,i} \cdot K_{f,i}}{n}$$

$$(17)$$

where n denotes the number of fracture stages; the subscript i

represents the *i*th fracturing stage; L_f denotes the half length of the fracture, m; W represents bandwidth of the fracturing stages; H represents the fracture height, m; α denotes the angle between the fracture and horizontal well, \circ ; W_f denotes fracture width, mm; K_f denotes fracture permeability, D.

3.4. Optimization and validation of the evaluation model

Since model calculation and prediction are the main function of the deep neural network, its performance impacts the model prediction results significantly. Therefore, the hyper-parameters and structure of the deep neural network need to be optimized, especially the number of hidden layers and neurons in each hidden layer. In addition, the model was validated with the method of k-fold cross-validation.

3.4.1. Optimization of the deep neural network

The number of neurons in each hidden layer significantly impacts the complexity and accuracy of the deep neural networks. Generally, the same number of neurons could be allocated to all hidden layers, whereas appropriate number of neurons in each hidden layer needs to be determined. Few neurons could result in model underfitting or high bias while overfitting or some other problems may occur with too many neurons. Specifically, too many neurons or too strong information processing capability of the neural network may result in unappropriated training of some neurons in the hidden layers and even model overfitting due to the limited information contained in the training data. In addition, even if enough information is contained in the training data, too many neurons in the hidden layers would increase the training time and difficulty of achieving the anticipated results. In consequence, the number of neurons in each hidden layer needs to be optimized.

The number of neurons in each hidden layer can be calculated according to the Kolmogorov's theorem for neural networks as follows:

$$m = (p+q)0.5 + c \tag{18}$$

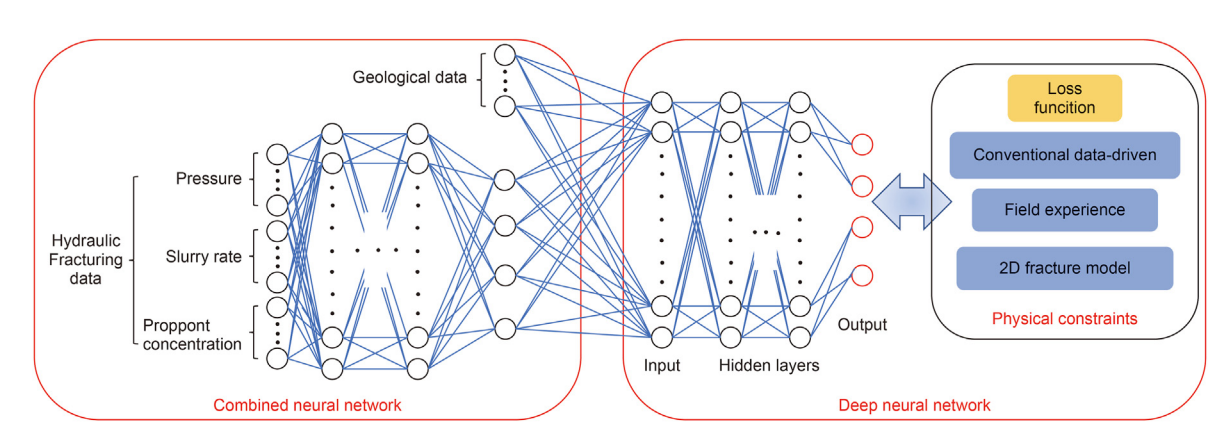


Fig. 4. The structure of the model of fracturing effect evaluation of horizontal well.

where m is the number of neurons in each hidden layer, p is the number of neurons in the input layer, q is the number of neurons in the output layer, and c is a constant ranging between 1 and 10. The optimal number of neurons in each hidden layer is determined as 60 after training and the RMSE of the model is 10.25.

Apart from the number of neurons in each hidden laver, the number of hidden layers also has a great impact on the performance and prediction results of the neural network model, which needs to be optimized. The performance of the model can be improved more significantly by increasing the number of hidden layers than that of the neurons in each hidden layer. In theory, the more hidden layers, the stronger the capability of the model prediction, and the better the prediction results. However, the increase in the number of hidden layers may result in overfitting, increasing the difficulty of model training and convergence. The number of hidden layers affects the accuracy of the model, as shown in Fig. 5. The model evaluation indicators of MSE and RMSE decrease all the time as the number of hidden layers increases from 2 to 5, with the minimum values of 60.11 and 7.75, respectively. They begin to increase as the number of hidden layers increases to 6, indicating that the model is inclined to overfit. Therefore, the optimal number of hidden layers is determined as 5 in this study.

3.4.2. K-fold cross-validation

Since the sample data set is relatively small in this study, the method of cross-validation was adopted to obtain as much effective information as possible from the limited data. Simple cross-validation is normally utilized by randomly dividing the sample data set into training set and test set. The model and parameters are trained with the training set and evaluated with the test set. The samples are then scrambled, the training set and test set are reselected to train and test the model. However, the model prediction results may still be bad with the simple cross-validation due to the inadequate data utilization.

In consequence, the k-fold cross-validation method was utilized to increase the rationality and accuracy of the model evaluation and k was determined as 10 in this study, as shown in Fig. 6. The total sample data were divided into 10 subsets with equal size, which were iterated over successively to validate the model. During each round of validation, the current sample data subset conducts as the test set while all the remaining subsets are the training set, and the model was trained and evaluated. In this study, there are 180 samples for the training set and 20 samples for the test set in each round. The average evaluation results of the 10 rounds of validation were regarded as the indicator of the model evaluation.

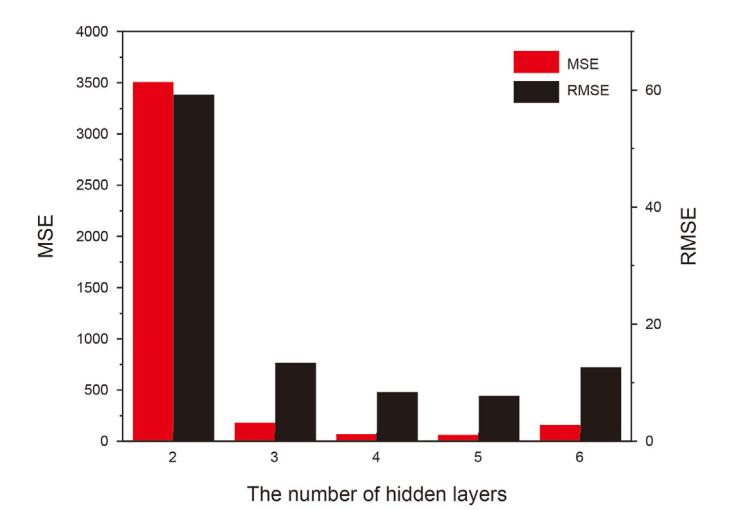


Fig. 5. Comparison of the MSE and RMSE for different numbers of hidden layers.

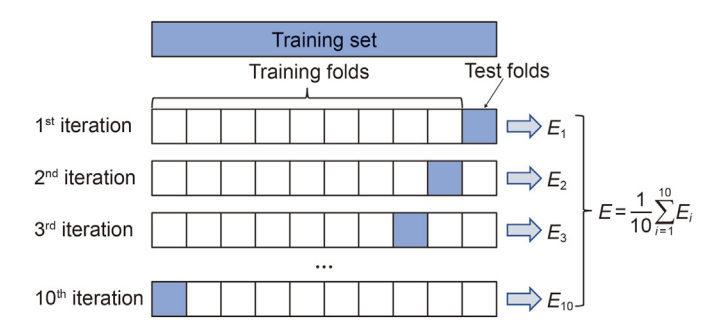


Fig. 6. The method of k-fold cross-validation (k = 10 in this study).

4. Results

In this section, the results of model training and test were illustrated and the fracture parameters were predicted with the validated model. In addition, the effects of the combined neural networks, physical constraints and method of *k*-fold cross-validation on the performance of the model of fracturing effect evaluation of horizontal wells were analyzed. Moreover, the model was applied to predict the fracture parameters of the well Y in the adjacent platform C and the prediction accuracy was evaluated according to the evaluation indicators.

4.1. Prediction results of the model of fracturing effect evaluation of horizontal wells

In this section, the performance of the model was evaluated and the fracture geometry parameters and fracture permeability were predicted based on the sample data set and the established model of fracturing effect evaluation of horizontal wells. The appropriate number of training times was optimized and determined as 300 according to the minimum final loss and RMSE after 10 rounds of validation. The model was validated with the method of 10-fold cross-validation according to the loss and prediction error, as shown in Fig. 7. The initial loss and RMSE of both training set and test set are pretty high in the first round of model validation, and decrease rapidly with the increase of training times. The loss and RMSE of the test set decrease more slowly than those of the training set with higher final values. After 10 rounds of validation, the performance of the test set is better with lower loss and RMSE, indicating that the 10-fold cross-validation can improve the model performance efficiently.

Specifically, in the first round of model validation, the loss of the training set decreases rapidly from 600 to 450 in the first 15 times of training and then decreases slowly to 350 with a constant rate. Similarly, the loss of the test set drops sharply from 800 to 230 in the first 15 times of test and then reduces slightly to 210, as shown in Fig. 7a. After ten rounds of validation, the loss of the training set and test set tends to be stable, slightly fluctuating around 58 and 37 respectively. The trend of the RMSE is similar to the loss, as shown in Fig. 7b. During the first round of model validation, the RMSE of the training set decreases rapidly from 45 to 15 in the first 10 times of training and barely changes thereafter. The RMSE of the test set reduces from 25 to 21 in the first 10 times of test, and then slowly decreases to 19. After ten rounds of validation, the RMSE of the training set and test set levels off, and slightly fluctuates around 7.6 and 6.1 respectively.

The fracture parameters of the whole sample set were predicted with the validated model and compared with the expected data, as shown in Fig. 8. The indicators of relative error, RMSE, MRE, and R^2 of the fracture length, fracture height, fracture width, and fracture

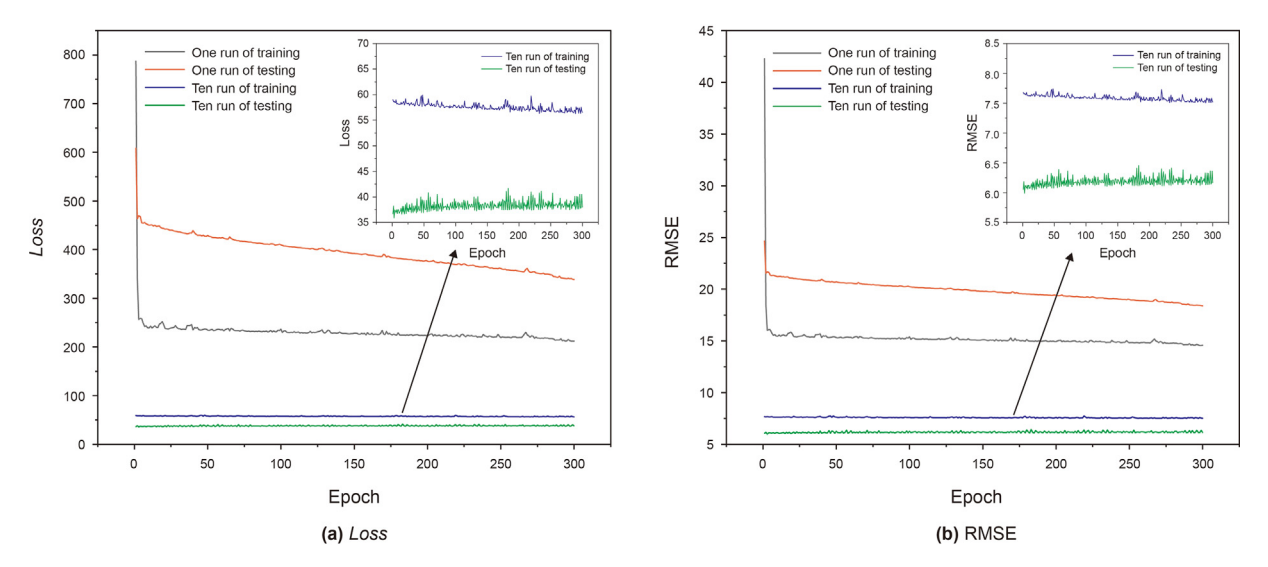


Fig. 7. Variations of the loss and RMSE with training times in the first and last rounds of 10-fold cross-validation.

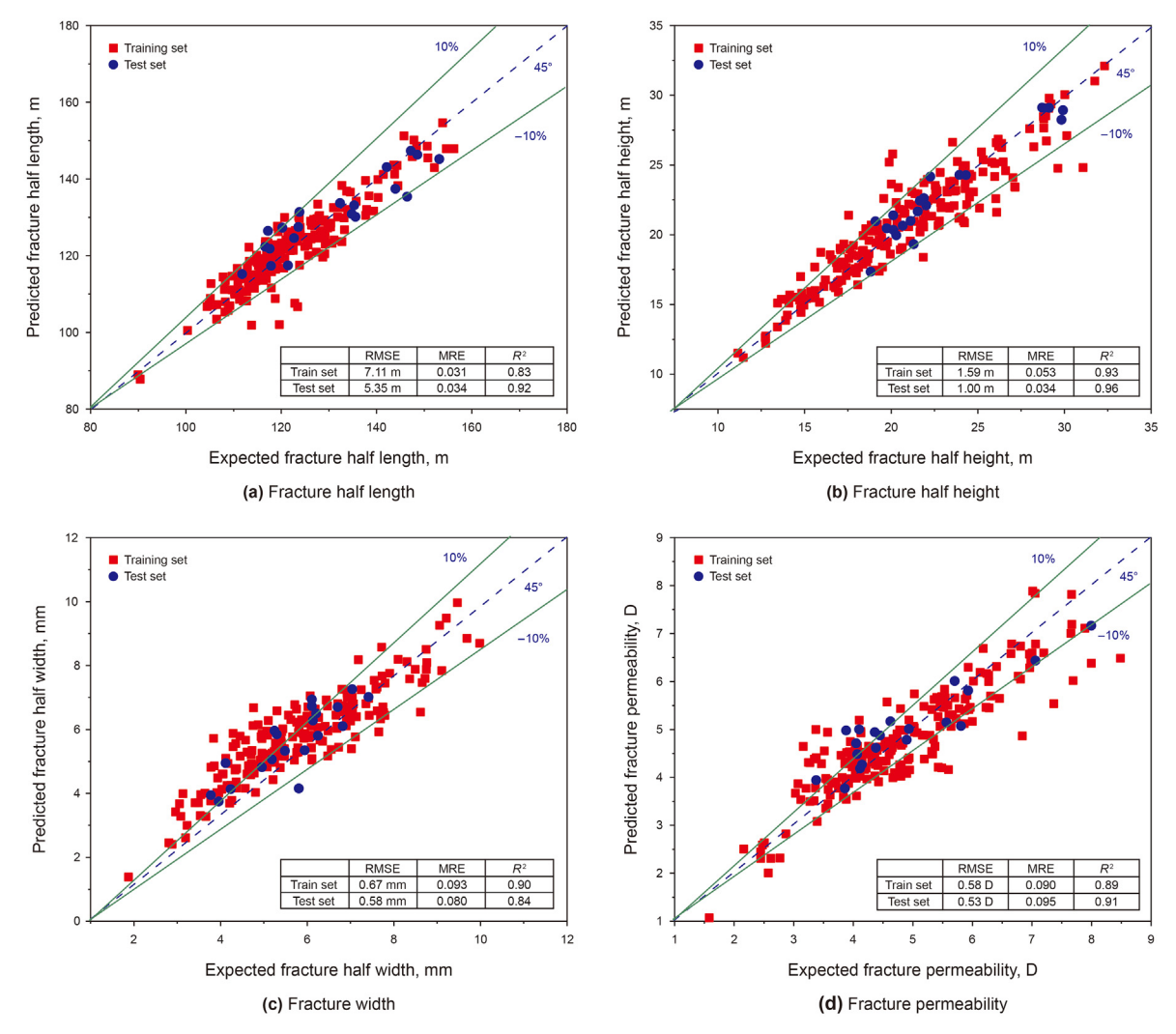


Fig. 8. Comparison of predicted and expected (true) values of the training set and test set (red data points for the training set, blue data points for the test set).

permeability were calculated respectively to evaluate the accuracy of the model prediction. The ideal results occur if the model prediction results are the same as the expected data, when the points fall on the 45° dotted line. In addition, the closer the data points to the 45° dotted line, the more accurate the model prediction.

The results indicate that relative errors of fracture geometry parameters and fracture permeability are under 10% by and large. and the majority of the data points lie between the two green lines representing the range of relative error of (-10%, 10%). In addition, the MRE of all fracture parameters are less than 0.1, and the values of R^2 are in the range between 0.83 and 0.96, indicating that the accuracy of the model prediction is fairly high. Specifically, the relative errors of fracture length and fracture height are under 10%, and the prediction accuracy of the test set is higher than that of the training set. The prediction errors of fracture width and fracture permeability are slightly higher due to the lower order of magnitude of the values. The smaller the parameters, the greater the errors. However, all the prediction errors are within the acceptable error range. The slightly higher errors of the fracture width and fracture permeability may also be caused by the input data. As mentioned above, fracture width and fracture permeability determine the fracture conductivity, which could not be diagnosed accurately with field monitoring technology. In this study, the fracture length and fracture height were calibrated with the field microseismic data while the calibration to fracture conductivity is relatively weak, which affects the prediction accuracy of the model to some extent.

According to the evaluation indicators calculated by Eqs. (8)–(10), the comprehensive fracturing effects of platform A were evaluated. The SRV, FCI and FC is 10191×10^4 m³, 0.41, and 28.1 D·cm respectively. Results demonstrate that the wells in platforms A are successfully stimulated. Therefore, the model proposed in this study can be applied to evaluate the fracturing effects.

4.2. Analysis of factors affecting the performance of the evaluation model of fracturing effects

4.2.1. Effects of the combined neural network

In this section, the prediction results of the test set of two models were compared by changing the neural network of the model input module while considering the same physical constraints and applying the same cross-validation method to the same sample data set. In addition, the impact of the combined deep neural network on the performance of the model of fracturing effect evaluation of horizontal wells was analyzed. The conventional convolutional neural network (CNN) and combined deep neural network (C-DNN) was utilized as the input module respectively while other settings are the same as those of the basic model. Since the same dimensional data should be input with CNN, the dynamic fracturing treatment data was chosen as the model input data of the CNN, whereas both static and dynamic data were adopted as the input data of the C-DNN.

The results illustrate that the prediction accuracy of the model is greatly improved with a 71.9% lower RMSE by inputting multidimensional data with C-DNN. The MRE of the fracture parameters predicted by the model with CNN is in the range between 0.16 and 0.29, as shown in Fig. 9, which decreases significantly with C-DNN with the highest value of 0.1, and the lowest value of 0.04. Specifically, the MRE of fracture length and fracture width decreases by 83.8% and 65.5% respectively. The excessive impact of dynamic data on the prediction results is diminished by inputting multiple types of data with C-DNN and adjusting the input network structure under the same physical constraints. In consequence, the prediction accuracy of fracture parameters is effectively improved.

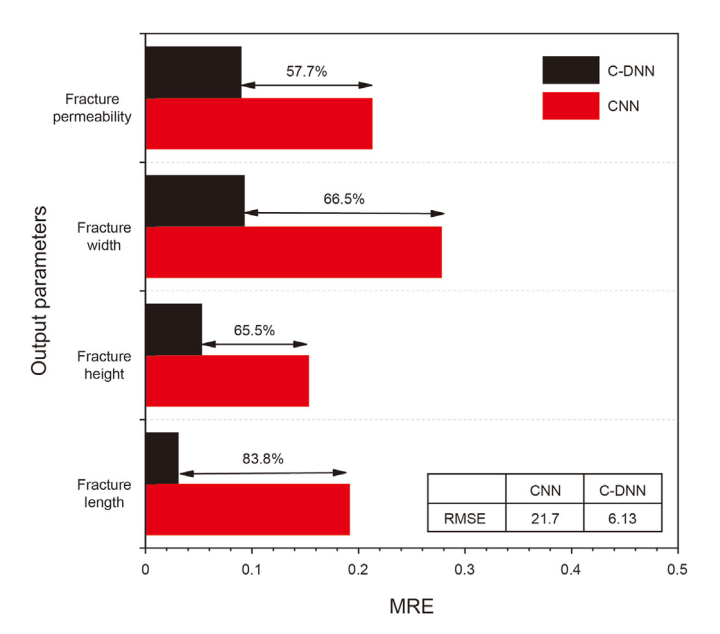


Fig. 9. Comparison of the mean relative error of prediction results using C-DNN and CNN as model input modules.

4.2.2. Effects of physical constraints

In this section, the prediction results of the test set of two models with and without physical constraints were compared by changing the loss function, and the impact of the physical constraints on the performance of the model of fracturing effect evaluation of horizontal wells was analyzed. The conventional datadriven loss function and the loss function considering physical constraints with field experience and the physical model of fracture parameters were adopted respectively. The other model settings are the same as those of the basic model. Both models were trained and validated with the same sample data set and 10-fold cross-validation method. The prediction results of models with conventional data-driven deep neural networks and deep neural networks considering physical constraints were compared.

The results indicate that the impact of physical constraints on the prediction results of the deep neural network is significant. The RMSE of the overall prediction results of fracture parameters decreases by 56% with consideration of physical constraints. In addition, the prediction is better because values of relative error between the prediction result and the expected data distribute more closely to 0. The relative errors of the data-driven model are large and distributed in the range of (-40%, 40%), denoted by the two red dotted lines, as shown in Fig. 10. The relative errors decrease after the physical constraints were incorporated and the distribution is narrowed down to the range between -10% and 10%, denoted by the two green dotted lines. Specifically, the MRE of the fracture length and fracture width predicted by the model with physical constraints reduces by approximately 75% respectively compared to that of the pure data-driven model, indicating that the performance of the model of the fracturing effect evaluation has been improved with the physical constraints considered.

4.2.3. Effects of k-fold cross-validation

In this section, the prediction results of three models were compared by changing the method of model validation. In addition, the impact of *k*-fold cross-validation on the performance of the model of fracturing effect evaluation of horizontal wells was analyzed. The model was trained first and validated with the methods of general validation, simple cross-validation (2-fold

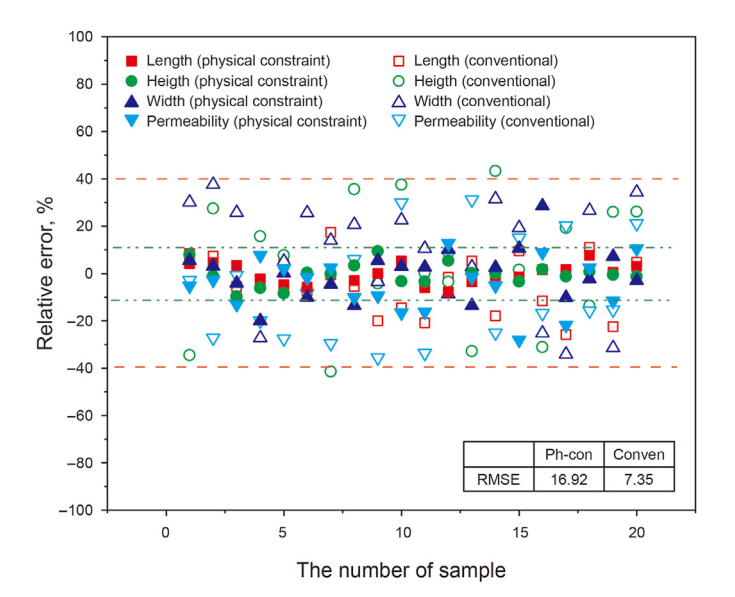


Fig. 10. Comparison of relative error distribution between two models with and without physical constraints (hollow data points represent the prediction results of conventional data-driven neural networks, and solid data points represent the prediction results of deep neural networks with physical constraints).

cross-validation), and *k*-fold cross-validation respectively, while other settings of the model and the sample data set are the same as those of the basic model.

The results demonstrate that the k-fold cross-validation method performs best, followed by the simple cross-validation, while the prediction accuracy of the model validated by the general validation method is the worst. Specifically, the MRE of the fracture parameters predicted by the model with general validation is between 0.45 and 0.53, as shown in Fig. 11, which decreases significantly with simple cross-validation ranging from 0.13 to 0.17, and further reduces to the range between 0.03 and 0.08 with the k-fold cross-validation.

In particular, the problem of overfitting is diminished by reducing the MRE of fracture height and fracture length by 80% and

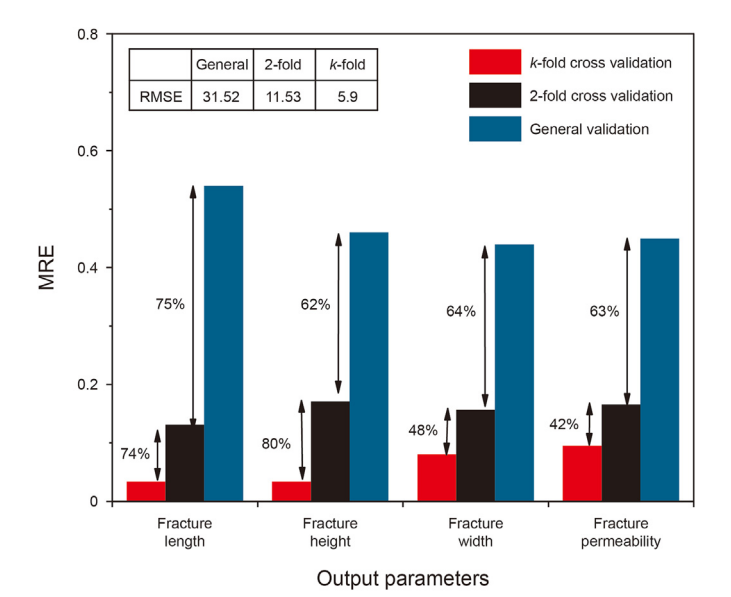


Fig. 11. Comparison of prediction results of models validated with the method of general validation, simple cross-validation, and *k*-fold cross-validation.

74% respectively. In consequence, the *k*-fold cross-validation can effectively improve the prediction accuracy of the model. The poor prediction performance with general validation results from the improper division of the training set and test set. The prediction results tend to be sensitive to certain data without cross-validation, which may lead to small error for the training set and large error for the test set and further result in overfitting. Nevertheless, more information can be obtained from fewer data with simple cross-validation and over-fitting can be avoided, while *k*-fold cross-validation performs better than the simple cross-validation by increasing the rounds of model training and testing to take full advantage of limited data. The irrationality of data set dividing is reduced and the prediction accuracy of the model with the small sample data set is considerably improved by applying the *k*-fold cross-validation in this study.

4.3. Field application

In this section, the model of fracturing effect evaluation of horizontal wells was applied to the well Y in the adjacent platform C to predict the fracture parameters. The indicators including the relative error (RE), root mean square error (RMSE), and average relative error (MRE) of the prediction results were calculated to evaluate the accuracy of the model.

Results indicate that the prediction of the fracture length is the best with relative errors basically ranging between -10% and 10%, while the predictions of fracture height, fracture width, and fracture permeability are pretty good with relative errors basically distributing in the range of (-15%, 15%), denoted by the two blue dotted lines, as shown in Fig. 12. The MRE of all the fracture parameters are approximately 0.1, demonstrating that the generalization ability of the evaluation model established in this study is fairly good. It can be used to predict the fracturing parameters of other horizontal wells in the block and evaluate the fracturing effects.

According to the evaluation indicators calculated by Eqs. (8)–(10), the comprehensive fracturing effects of well Y in platform C were evaluated. The SRV, FCI and FC of well Y in platform C is $570.6 \times 10^4 \, \text{m}^3$, 0.63, and 70.13 D·cm respectively. The results indicate that the fracture of well Y in platform C is more complex with higher conductivity while the SRV of 8 wells in platform A is much larger.

5. Conclusions

In this study, a model based on the deep neural network considering physical constraints was presented to evaluate the fracturing effects of horizontal wells in tight oil and gas reservoirs. In addition, the field experience and KGD fracture calculation model were incorporated in the loss function as physical constraints. Moreover, the model performance was improved by optimizing the deep neural network and adopting the *k*-fold cross-validation. Some main conclusions were drawn as follows.

- (1) The number of hidden layers and neurons in each hidden layer in the deep neural network impact the model performance significantly, which was optimized as 5 and 60 respectively. The more the number of hidden layers and neurons, the more complex the model and the easier the model was over-fitted.
- (2) The evaluation model performs well in fracture parameters prediction and generalization. The adoption of physical constraints and *k*-fold cross-validation effectively improves the prediction accuracy of the model. The relative errors of fracture parameters are basically within 10%.

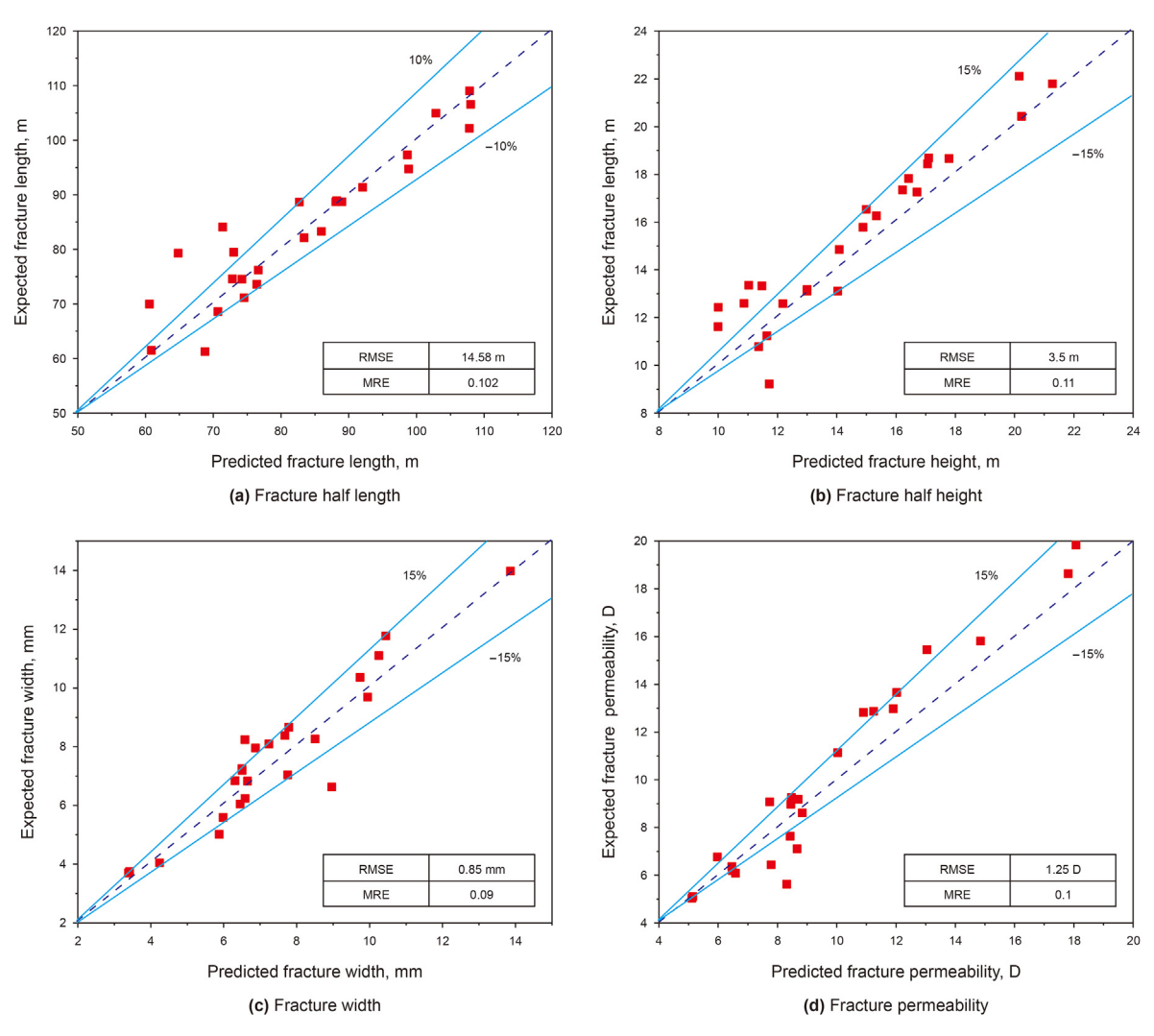


Fig. 12. Prediction results of fracture parameters of well Y in platform C.

(3) The combination of two neural networks effectively improves the model performance, considerably reducing the root-mean-square error. The combined neural network improvs the impact of static data on prediction results and reduces the RMSE of the model by 71.9%.

Declaration of competing interest

The authors declare that they have no known competing financial interests or personal relationships that could have appeared to influence the work reported in this paper.

Acknowledgments

This work is supported by the National Natural Science Foundation of China (Grant No. 52174044, 52004302), Science Foundation of China University of Petroleum, Beijing (No. ZX20200134, 2462021YXZZ012), and the Strategic Cooperation Technology Projects of CNPC and CUPB (ZLZX 2020-01-07).

References

Barree, R.D., Barree, V.L., Craig, D.P., 2009. Holistic fracture diagnostics: consistent interpretation of prefrac injection tests using multiple analysis methods. SPE Prod. Oper. 24, 396–406. https://doi.org/10.2118/107877-PA. Chen, Y., Saad, O.M., et al., 2022. 3D microseismic monitoring using machine learning. J. Geophys. Res. Solid Earth 127 (3), e2021JB023842. https://doi.org/ 10.1029/2021JB023842.

Cheng, Y., Fu, L.Y., 2022. Nonlinear seismic inversion by physics-informed Caianiello convolutional neural networks for overpressure prediction of source rocks in the offshore Xihu depression, East China. J. Petrol. Sci. Eng. 215 (Part B), 110654. https://doi.org/10.1016/j.petrol.2022.110654.

Cipolla, C.L., Warpinski, N.R., Mayerhofer, et al., 2008. The Relationship between Fracture Complexity, Reservoir Properties, and Fracture Treatment Design. SPE Annual Technical Conference and Exhibition, Denver, Colorado, USA. https://doi.org/10.2118/115769-MS.

Dong, Y., Song, L., Zhang, Y., et al., 2022. Initial productivity prediction method for offshore oil wells based on data mining algorithm with physical constraints. Editorial Department of Petroleum Geology and Recovery Efficiency 29 (1), 137–144. https://doi.org/10.13673/j.cnki.cn37-1359/te.2022.01.017.

Esfandiari, M., Pak, A., 2023. XFEM modeling of the effect of in-situ stresses on hydraulic fracture characteristics and comparison with KGD and PKN models. J. Pet. Explor. Prod. Technol. 13 (1), 185–201. https://doi.org/10.1007/s13202-022-01545-7.

Fiallos Torres, M., Morales, A., Yu, W., et al., 2021. Characterization of complex hydraulic fractures in Eagle Ford shale oil development through embedded discrete fracture modeling. Petrol. Explor. Dev. 48 (3), 713–720. https://doi.org/10.1016/s1876-3804(21)60057-5.

Fries, T.P., Belytschko, T., 2010. The extended/generalized finite element method: an overview of the method and its applications. Int. J. Numer. Methods Eng. 84 (3), 253–304. https://doi.org/10.1002/nme.2914.

He, Y., Song, Z., Zhang, Y., et al., 2021. Review on application of machine learning in hydraulic fracturing. Journal of China University of Petroleum (Edition of Natural Science) 45 (6), 127–135. https://doi.org/10.3969/j.issn.1673-5005.2021.06.015 (in Chinese).

Huang, W.L., Gao, F., Liao, J.P., et al., 2020. A deep learning network for estimation of

- seismic local slopes. Petrol. Sci. 18 (1), 92–105. https://doi.org/10.1007/s12182-020-00530-1.
- Janiesch, C., Zschech, P., Heinrich, K., 2021. Machine learning and deep learning. Electron. Mark. 31 (3), 685–695. https://doi.org/10.1007/s12525-021-00475-2.
- Jaripatke, O.A., Barman, I., Ndungu, J.G., et al., 2018. Review of Permian completion designs and results. In: Proceedings of SPE Annual Technical Conference and Exhibition, Dallas, Texas, USA. https://doi.org/10.2118/191560-MS.
- Kulga, B., Artun, E., Ertekin, T., 2018. Characterization of tight-gas sand reservoirs from horizontal-well performance data using an inverse neural network. J. Nat. Gas Sci. Eng. 59, 35—46. https://doi.org/10.1016/j.jngse.2018.08.017.
- Lei, Q., Weng, D., Xiong, S., et al., 2021. Progress and development directions of shale oil reservoir stimulation technology of China National Petroleum Corporation. Petrol. Explor. Dev. 48 (5), 1198–1207. https://doi.org/10.1016/S1876-3804(21) 60102-7
- Lei, Q., Xu, Y., Cai, B., et al., 2022. Progress and prospects of horizontal well fracturing technology for shale oil and gas reservoirs. Petrol. Explor. Dev. 49 (1), 191–199. https://doi.org/10.1016/s1876-3804(22)60015-6.
- Li, D., Yang, R., Zhang, D., et al., 2019. Distribution trend analysis of hydraulic fracturing events: taking MY1 Well microseismic monitoring as an example. Fault-Block Oil Gas Field 26 (3), 346–349. https://doi.org/10.13686/i.cnki.dzvzv.2022.01.013.
- Li, G., Qin, J., Xian, C., et al., 2020. Theoretical understandings, key technologies and practices of tight conglomerate oilfield efficient development: a case study of the Mahu Oilfield, Junggar Basin, NW China. Petrol. Explor. Dev. 47 (6), 1275—1290. https://doi.org/10.1016/S1876-3804(20)60135-0.
- Li, J., Yu, B.S., Tian, Y.K., et al., 2020. Effect analysis of borehole microseismic monitoring technology on shale gas fracturing in western Hubei. Appl. Geophys. 17, 764–775. https://doi.org/10.1007/s11770-020-0868-9.
- Liu, L., Song, W., Wang, H., et al., 2020. Hydraulic fracturing micro-seismic experiment study. Prog. Geophys. 35 (3), 852–858 (in Chinese).
- Liu, X.Y., Zhou, L., Chen, X.H., et al., 2020. Lithofacies identification using support vector machine based on local deep multi-kernel learning. Petrol. Sci. 17 (4), 954–966. https://doi.org/10.1007/s12182-020-00474-6.
- Mahmoud, A., Gowida, A., Aljawad, M.S., et al., 2021. Advancement of hydraulic fracture diagnostics in unconventional formations. Geofluids 2021, 4223858. https://doi.org/10.1155/2021/4223858.
- Miao, S., Zhang, H., Chen, Y., et al., 2019. Surface microseismic monitoring of shale gas hydraulic fracturing based on microseismic location and tomography. Geophys. Prospect. Pet. 58 (2), 262–271+284 (in Chinese).
- Pakhotina, I., Sakaida, S., Zhu, D., et al., 2020. Diagnosing multistage fracture treatments with distributed fiber-optic sensors. SPE Prod. Oper. 35 (4). https:// doi.org/10.2118/199723-PA, 0852-0864.
- Sang, K.H., Yin, X.Y., Zhang, F.C., 2021. Machine learning seismic reservoir prediction method based on virtual sample generation. Petrol. Sci. 18 (6), 1662–1674. https://doi.org/10.1016/j.petsci.2021.09.034.
- Shauer, N., Duarte, C.A., 2019. Improved algorithms for generalized finite element simulations of three-dimensional hydraulic fracture propagation. Int. J. Numer. Anal. Methods GeoMech. 43 (18), 2707–2742. https://doi.org/10.1002/nag.2977.

- Shrestha, A., Mahmood, A., 2019. Review of deep learning algorithms and architectures. IEEE Access 7, 53040–53065. https://doi.org/10.1109/access.2019.2912200.
- Soleimani, M., 2017. Naturally fractured hydrocarbon reservoir simulation by elastic fracture modeling. Petrol. Sci. 14 (2), 286–301. https://doi.org/10.1007/s12182-017-0162-5
- Song, H., Du, S., Yang, J., et al., 2022. Evaluation of hydraulic fracturing effect on coalbed methane reservoir based on deep learning method considering physical constraints. J. Petrol. Sci. Eng. 212, 110360. https://doi.org/10.1016/ j.petrol.2022.110360.
- Syed, F.I., Muther, T., Dahaghi, A.K., et al., 2022. CO₂ EOR performance evaluation in an unconventional reservoir through mechanistic constrained proxy modeling. Fuel 310, 122390. https://doi.org/10.1016/j.fuel.2021.122390.
- Tian, W., Wu, X., Shen, T., et al., 2016. Estimation of hydraulic fracture volume utilizing partitioning chemical tracer in shale gas formation. J. Nat. Gas Sci. Eng. 33, 1069–1077. https://doi.org/10.1016/j.jngse.2016.06.018.
- Tripoppoom, S., Xie, J., Yong, R., et al., 2020. Investigation of different production performances in shale gas wells using assisted history matching: hydraulic fractures and reservoir characterization from production data. Fuel 267, 117097. https://doi.org/10.1016/j.fuel.2020.117097.
- Valle dos Santos, RdO., Vellasco, M.M.B.R., 2015. Neural expert weighting: a new framework for dynamic forecast combination. Expert Syst. Appl. 42 (22), 8625–8636. https://doi.org/10.1016/j.eswa.2015.07.017.
- Wallace, J., Kabir, C.S., Cipolla, C., 2016. Probing diagnostic fracture injection tests in unconventional reservoirs. J. Petrol. Sci. Eng. 143, 245–257. https://doi.org/ 10.1016/j.petrol.2016.01.039.
- Wang, H., Alkhalifah, T., Waheed, U., et al., 2022. Data-driven microseismic event localization: an application to the Oklahoma Arkoma Basin hydraulic fracturing data. IEEE Trans. Geosci. Rem. Sens. 60, 1–12. https://doi.org/10.1109/tgrs.2021.3120546.
- Wu, J., Yin, X., Xiao, H., 2018. Seeing permeability from images: fast prediction with convolutional neural networks. Sci. Bull. 63 (18), 1215—1222. https://doi.org/ 10.1016/j.scib.2018.08.006.
- Xiao, J., Ke, X., Wu, H., et al., 2021. Production decline analysis and hydraulic fracture network interpretation method for shale gas with consideration of fracturing fluid flowback data. Geofluids 2021, 1—9. https://doi.org/10.1155/2021/6076566.
- Yang, R., Huang, Z., Li, G., et al., 2017. A semianalytical approach to model two-phase flowback of shale-gas wells with complex-fracture-network geometries. SPE J. 22 (6), 1808–1833. https://doi.org/10.2118/181766-PA.
- Zhang, K., Ma, X., Li, Y., et al., 2018. Parameter prediction of hydraulic fracture for tight reservoir based on micro-seismic and history matching. Fractals 26 (2), 1840009. https://doi.org/10.1142/s0218348x18400091.
- Zhao, J., Fu, Y., Wang, Z., et al., 2022. Diagnosis model of shale gas fracture network fracturing operation pressure curves. Nat. Gas. Ind. B. 9 (5), 448–456. https://doi.org/10.1016/j.ngib.2022.10.003.
- Zhou, J., Zhang, B., Li, K., et al., 2015. Fracture monitoring technology based on surface tiltmeter in well factor fracturing. Petroleum Drilling Techniques 43 (3), 71–75. https://doi.org/10.11911/syztjs.201503014.